TWO-CHANNEL SAR GROUND MOVING TARGET INDICATION FOR TRAFFIC MONITORING IN URBAN TERRAIN

I. Sikaneta and C. H. Gierull*

Defence R&D Canada – Ottawa
Radar Systems Section
3701 Carling Ave., Ottawa, ON, Canada, K1A 0Z4
E-mail: ishuwa.sikaneta@drdc-rddc.gc.ca

KEY WORDS: SAR, SAR-GMTI, Traffic Monitoring

ABSTRACT:

This paper introduces and analyses a technique that implements CFAR detection and parameter estimation of moving targets in urban terrain. Firstly, it presents a probability distribution to use with the product model. This model helps to account for the extremely high inhomogeneity encountered in urban terrain. Along with the proposed distribution, the paper then discusses the numerical computation of the CFAR thresholds for an arbitrary GMTI detection metric. For illustration, results have been generated using DPCA as the GMTI metric.

Unfortunately, having achieved CFAR for a small probability of false alarm, one finds that the probability of detection has decreased. To counter this, we propose to increase the target SCR by using a SAR processing filterbank where filters in the bank are designed to enhance moving targets since an increase in SCR improves detection [11, 3]. Following the filterbank operation, we construct a master target list of redundant information about the individual targets. This information is then exploited in a quasi-optimal manner to estimate the target velocities and locations while filtering out false alarms that have passed the CFAR test.

1. INTRODUCTION

In many civilian and military applications of airborne and spaceborne SAR imaging, it is highly desirable to simultaneously monitor ground traffic. The measurement of object motion using SAR requires two consecutive operations. Firstly, the detection in the SAR data and, secondly, target parameter estimation such as of location, speed and trajectory. Target detection and estimation can either be performed incoherently with a single SAR sensor, or coherently, with much higher fidelity, with two or more apertures. While many authors have investigated the detection part, the estimation part has only rarely been treated.

2. IMPLEMENTATION OF AUTOMATIC DETECTION ALGORITHMS

The detection of moving targets hinges upon the ability to distinguish these targets from clutter. As discussed in [9], one way of achieving clutter cancellation is to ensure that the clutter occupies only a well defined fraction of the available bandwidth of the system leaving moving targets in the remaining regions. An automatic implementation of this algorithm involves identifying and suppressing the clutter band. The residue data are then SAR processed and thresholded in power [9]. With a SAR system that oversamples in the Doppler direction, this approach can help to increase the target SCR by applying a SAR filter that has a Doppler bandwidth that only partly covers the clutter bandwidth. This assumes, correctly, that moving targets have bandwidths that also only partly cover the clutter band [9].

With a two-aperture system, clutter cancellation can be achieved by making use of the high correlation between the two antenna samples. We can write the complex slow time samples from the leading antenna and trailing antenna as $Z_1(m)$ and $Z_2(m)$, respectively. If necessary, and if the antenna samples are adequately sampled, we can interpolate the samples from the trailing antenna so that one estimates what it would have measured from the the measurement positions of the leading antenna. One thus estimates $Z_2(m+\Delta t)$, where Δt is the time required for the radar platform to move the trailing antenna into the former position of the leading antenna. The remainder of this paper assumes that $Z_2(m+\Delta t)$ has been estimated, and we simply write $Z_2(m)$ to represent $Z_2(m+\Delta t)$. If the channel samples are arranged as a vector,

$$\vec{Z}(m) = \begin{bmatrix} Z_1(m) \\ Z_2(m) \end{bmatrix} \tag{1}$$

and if the covariance matrix has the form,

$$\boldsymbol{R} = \begin{bmatrix} \sigma_1^2 & \sigma_1\sigma_2\rho \\ \sigma_1\sigma_2\rho & \sigma_2^2 \end{bmatrix}, \tag{2}$$

where σ_1^2 and σ_1^2 are the powers of the two antenna measurements, and where $0 \leq \rho \leq 1$ is a real correlation co-

efficient, then one method to detect the targets is to apply the linear filter and detector

$$Y(m) = |\vec{e}^{\dagger}\vec{Z}(m)|^2, \tag{3}$$

where † denotes the Hermitian transpose and where the $2-$element vector, $\vec{e}$, serves to provide a weighted sum of the antenna samples. It should be chosen to maximise the moving target SCR. Additionally, one can average neighbouring samples in the data space with the effect of reducing clutter variance (increasing SCR) at the expense of resolution. Often, averaging is referred to as "multi-looking"; hence, a n-look sample consists of the average of n independent samples.

The implementation of an automatic CFAR algorithm requires applying a threshold to $Y(m)$. This threshold depends on the statistics of the random vectors $\vec{Z}(m)$. The majority of the literature considers $\vec{Z}(m)$ to be a locally stationary complex, zero-mean Gaussian vector[1] allowing the complex Wishart distribution of the sample covariance matrix estimates to be applied [14, 8, 1]. We consider the sample covariance matrix defined by

$$\hat{\boldsymbol{R}} = \sum_{m=0}^{n-1} \vec{Z}(m)\vec{Z}^{\dagger}(m) \tag{4}$$

because, as demonstrated in [11], most GMTI metrics, such as DPCA and the ATI phase among others, are computable from it.

In the 2-channel case, when the data from each are balanced in power, the linear filter approach leads to DPCA. It has been shown that in homogeneous terrain, DPCA is the optimal filter for GMTI [4]. DPCA prescribes that $\vec{e}^{\dagger} = [1\ -1]$, therefore,

$$Y = \sum_{m=0}^{n-1} |Z_1(m) - Z_2(m)|^2. \tag{5}$$

Physically, DPCA relies upon the expectation that two time displaced measurements of a static target will yield two identical results. Thus, after subtraction, the metric should return zero. However, if the target does change between measurements, for example due to a motion-induced phase, or because of white receiver noise, then the subtraction will yield a non-zero result.

As the difference of the two statistically dependent complex Gaussian random variables in (5) is again normal distributed with zero mean and variance

$$\sigma_{\Delta}^2 = \sigma_1^2 + \sigma_2^2 - 2\rho\sigma_1\sigma_2, \tag{6}$$

Y is χ^2 distributed with density

$$f_Y(y) = \frac{y^{n-1}}{\Gamma(n)\sigma_{\Delta}^{2n}} \exp\left(-y/\sigma_{\Delta}^2\right). \tag{7}$$

[1] this corresponds to homogeneous terrain

In another approach, specific to a 2-channel system, the phase of one of the off-diagonals of the covariance matrix estimate is used as a detector. The off-diagonal elements are the product of one channel and the complex conjugate of the other. The resulting quantity is referred to as the interferogram [9]. The rationale for this approach considers the physical differences between the two time-delayed snapshots of the target under observation. If a target moves through in the range direction between the snapshots from the two apertures, then the corresponding difference in range will manifest as a proportional difference in phase. This phase measurement divided by the displacement time can provide an estimate of the target radial velocity. However, considering detection, since most of the terrain has not changed, the phase difference between measurements should be zero. It should be emphasised that the data are not linearly filtered as in DPCA. Implementation of the automatic phase detector requires calculation of the phase distribution of the interferogram. This has been done, for example, by using the complex Wishart distribution [8]. The multi-looked interferometric phase is computed as

$$\delta = \arg\left(\sum_{m=0}^{n-1} Z_1^*(m)Z_2(m)\right). \tag{8}$$

The statistical properties of δ in homogeneous terrain have been extensively investigated [2, 7, 8, 14].

3. MULTIPLICATIVE TEXTURE RANDOM VARIABLE

In practice, one often encounters limitations in the model of a stationary zero-mean Gaussian process in each channel. Although the stationary Gaussian model is still locally suitable, the process is not stationary when the background reflectivity (variance) changes from multilooked sample to multilooked sample. While it is still valid to assume that the mean of the process is zero and stationary, the variance must be modelled as globally non-stationary. For instance, the variance of the SAR data may be quite different for grassy terrain as compared to forested terrain. In a scene containing both types (and more) of terrain, a statistical description of the random variance must be included to validate the model.

To this end, the introduction of a random variable $A \in [0, \infty)$ such that $\hat{\boldsymbol{R}} \to A\hat{\boldsymbol{R}}$, leads to the so-called product model. Many authors have studied appropriate statistical models for A including [14, 7, 1]. This paper adopts the inverse chi-square model, χ^{-2}, of [1], with a generalisation to arbitrary powers, $\chi^{-2\kappa}$, $\kappa > 0$. The probability density function for χ^{-2} is given by [1]

$$f_A(a) = \frac{\Theta^{\nu} e^{-\Theta/a}}{\Gamma(\nu)a^{\nu+1}}, \quad a \in [0, \infty), \tag{9}$$

where Θ and ν are the shape and degree of freedom parameters, respectively. It also has a cumulative distribution function given by

$$F_A(a) = \frac{1}{\Gamma(\nu)}\Gamma(\nu, \Theta/a), \tag{10}$$

which can readily be computed from the characteristic function for the gamma function presented in [13]. Imposing the constraint $\mathcal{E}_A\{A\} = 1$[2] introduces a dependence between the two parameters of the distribution; thereby, effectively, leaving only a single describing parameter. In the case of (9), the constraint yields $\Theta = \nu - 1$.

In our proposed generalisation of the above random variable, we make the transformation $A \rightarrow W = A^\kappa$ where $\kappa > 0$. The Jacobian introduced by this transformation is $\mathrm{d}w = \kappa a^{\kappa-1}\mathrm{d}a$ thus leading to a probability distribution for W given by

$$f_W(w) = \frac{(\nu-1)^\nu e^{-\frac{\nu-1}{w^{1/\kappa}}}}{\kappa\Gamma(\nu)w^{\nu/\kappa+1}} \tag{11}$$

Generally, the theoretical distribution generated assuming homogeneous conditions predicts fewer high valued samples than are actually measured. The purpose of the random variable, W, is thus to elongate the theoretical probability distribution.

The introduction of the product model complicates evaluation of closed form solutions of the theoretical probability distributions. However, closed form solutions can be specified for the classical techniques of ATI and DPCA. For the ATI phase it is easy to verify that the common multiplier W for the real and imaginary components in (8) cancels out when the argument is computed [2, 7, 8, 14]. In other words, the ATI phase for the clutter is invariant against the multiplicative texture random variable and hence, determination of the CFAR threshold remains unchanged from the homogeneous case.

For DPCA we have

$$Z = W \cdot Y = W \sum_{m=0}^{n-1} |Z_1(m) - Z_2(m)|^2, \tag{12}$$

the pdf of (12), for the special case of $\kappa = 1$, can be calculated as

$$\begin{aligned} f_Z(z) &= \int_0^\infty \frac{1}{w} f_W(w) f_Y(\frac{z}{w})\, dw \\ &= \frac{[(\nu-1)\sigma_\Delta^2]^\nu}{B(n,\nu)} \frac{z^{n-1}}{[(\nu-1)\sigma_\Delta^2 + z]^{n+\nu}}, \end{aligned} \tag{13}$$

[2] $\mathcal{E}_X\{\cdot\}$ denotes expectation relative to X

where $B(n,\nu) = \Gamma(n)\Gamma(\nu)/\Gamma(n+\nu)$. The r^{th} moment of Z is

$$\mathcal{E}_Z\{Z^r\} = [(\nu-1)\sigma_\Delta^2]^r \frac{B(n+r, \nu-r)}{B(n,\nu)} \qquad \nu > r, \tag{14}$$

which can be exploited to estimate the parameter ν within a given SAR data set [2]. The cumulative probability function can be derived as

$$F_Z(z) = \frac{z^n}{n[(\nu-1)\sigma_\Delta^2]^n} {}_2\mathrm{F}_1(n+\nu, n; n+1; -\frac{z}{(\nu-1)\sigma_\Delta^2}), \tag{15}$$

where ${}_2\mathrm{F}_1(a, b; c; z)$ is the Gauss hypergeometric function, [6]. Using [10], the characteristic function can be expressed as

$$\begin{aligned} \phi_Z(s) &= {}_1\mathrm{F}_1(n, 1-\nu; -js(\nu-1)\sigma_\Delta^2) \\ &\quad + \frac{\Gamma(-\nu)(-js(\nu-1)\sigma_\Delta^2)^\nu}{\Gamma(n+\nu)} \\ &\quad \cdot {}_1\mathrm{F}_1(n+\nu, 1+\nu; -js(\nu-1)\sigma_\Delta^2), \end{aligned} \tag{16}$$

which is valid for $\nu \in \mathcal{R}^+$ by analytic continuation.

In general, closed form expressions for the pdf of arbitrary amplitude-dependent GMTI metrics are more elusive. This paper therefore presents a method for numerically computing the distribution functions.

4. NUMERICAL METHODS FOR THE GENERAL PRODUCT MODEL

The model for non-negative power dependent metrics such as DPCA assumes statistical independence in the texture statistic. Let us designate an arbitrary non-negative power dependent random variable as X. In the previous section we had $X = Y$, the random variable describing DPCA. We seek the probability distribution for $Z = WX$. Since $W > 0$ and $X > 0$,

$$F_Z(z) = \mathcal{E}_X\{F_W(z/X)\}, \tag{17}$$

where $\mathcal{E}_X\{\cdot\}$ denotes expectation relative to the random variable x, one finds that

$$f_Z(z) = \mathcal{E}_X\{f_W(z/X)\frac{1}{X}\}. \tag{18}$$

Computation of the threshold, δ_z, for a CFAR detector with false alarm rate P_F, requires solving $1 - F_Z(\delta_z) = \mathrm{P}_F$.

We now focus on the chosen probability distribution for W, namely,

$$\begin{aligned} F_W(w) &= F_A(w^{1/\kappa}) \\ &= \frac{1}{\Gamma(\nu)}\Gamma(\nu, \Theta/(w^{1/\kappa})). \end{aligned} \tag{19}$$

Using (18), one finds that

$$F_Z(z) = \int_0^\infty \frac{\Gamma(\nu, \Theta(x/z)^{1/\kappa})}{\Gamma(\nu)} \mathrm{d}F_X(x), \qquad (20)$$

where, for the cases that we generally consider, $\mathrm{d}F_X(x) = f_X(x)\mathrm{d}x$. Evaluation of the CFAR threshold requires solving

$$\mathrm{P}_F = 1 - \int_0^\infty \frac{\Gamma(\nu, \Theta(x/\delta_z)^{1/\kappa})}{\Gamma(\nu)} \mathrm{d}F_X(x) \qquad (21)$$

for δ_z. Section 5. shows that

$$\mathcal{E}_W\{W\} \equiv 1 \Rightarrow \Theta \equiv \left(\frac{\Gamma(\nu)}{\Gamma(\nu-\kappa)}\right)^{1/\kappa}, \qquad (22)$$

therefore, a further simplification of (21) leads to

$$\mathrm{P}_F = 1 - \int_0^\infty \frac{\Gamma\left(\nu, \left[\frac{x\Gamma(\nu)}{\delta_z\Gamma(\nu-\kappa)}\right]^{1/\kappa}\right)}{\Gamma(\nu)} \mathrm{d}F_X(x) \qquad (23)$$

To solve (23) one requires an estimate of ν and κ. Estimation of these parameters is discussed in section 5.. Once these parameters have been determined, numerical integration can be performed on (23) using the distribution for X where appropriate. For example, if X corresponds to DPCA, we substitute the pdf for DPCA into (23) and solve for δ_z [11].

5. METHOD FOR ESTIMATING TEXTURE VARIABLE PARAMETERS

This section outlines a method for estimating the texture variable parameters necessary for the construction of the texture pdf. The following assumption sets up the solution: the complex random variable measured by each antenna of the radar is the product of a sum of zero-mean complex Gaussian variables, each with variance σ^2, and a χ^{-2} random variable raised to the power κ.

Consider

$$Z = A^\kappa \sum_{m=0}^{n-1} U(m), \qquad (24)$$

where $U(m) = |Z_1(m)|^2$ is the squared envelope of the circular complex Gaussian random variable measured by the fore antenna, and A is χ^{-2} distributed. Let us compute $\mathcal{E}_Z\{Z^r\}$. Since A and $U(m)$ are assumed to be statistically independent,

$$\mathcal{E}_Z\{Z^r\} = \mathcal{E}_A\{A^{\kappa r}\}\mathcal{E}_U\left\{\left(\sum_{m=0}^{n-1} U(m)\right)^r\right\}. \qquad (25)$$

With each $U(m)$ independently identically χ^2 distributed, we have seen from (7) that the sum, $V = \sum_{m=0}^{n-1} U(m)$, has probability distribution

$$f_V(v) = \frac{v^{n-1}e^{-v/\sigma^2}}{\Gamma(n)(\sigma^2)^n}, \qquad (26)$$

with expected value

$$\begin{aligned}\mathcal{E}_V\{V^r\} &= \int_0^\infty v^r \frac{v^{n-1}e^{-v/\sigma^2}}{\Gamma(n)(\sigma^2)^n}\mathrm{d}v \\ &= \frac{(\sigma^2)^r}{\Gamma(n)}\int_0^\infty \left(\frac{v}{\sigma^2}\right)^{n+r-1} e^{-v/\sigma^2}\mathrm{d}\frac{v}{\sigma^2} \\ &= \frac{\Gamma(r+n)(\sigma^2)^r}{\Gamma(n)}.\end{aligned} \qquad (27)$$

By using (9), we see that the moments of A^κ are

$$\begin{aligned}\mathcal{E}_A\{A^{\kappa r}\} &= \int_0^\infty \frac{a^{\kappa r}\Theta^\nu e^{-\Theta/a}}{\Gamma(\nu)a^{\nu+1}}\mathrm{d}a \\ &= \frac{\Theta^{\kappa r}}{\Gamma(\nu)}\int_0^\infty t^{\nu-\kappa r-1}\exp(-t)\mathrm{d}t \\ &= \frac{\Theta^{\kappa r}\Gamma(\nu-\kappa r)}{\Gamma(\nu)}.\end{aligned} \qquad (28)$$

The second line above makes the substitution $t = \Theta/a$. Requiring that $\mathcal{E}_A\{A^\kappa\} = 1$ dictates that $\Gamma(\nu) = \Theta^\kappa\Gamma(\nu-\kappa)$, or $\Theta = [\Gamma(\nu)/\Gamma(\nu-\kappa)]^{1/\kappa}$. Substituting (27) and (28) into (25) yields

$$\mathcal{E}_Z\{Z^r\} = \frac{\sigma^{2r}\Gamma(n+r)}{\Gamma(n)}\left[\frac{\Gamma(\nu)}{\Gamma(\nu-\kappa)}\right]^r \frac{\Gamma(\nu-\kappa r)}{\Gamma(\nu)}. \qquad (29)$$

For moderately heterogeneous terrain, the appropriate choice for κ, empirically, seems to be $\kappa = 0.5$. Instances of $\kappa = 1$ have been observed for grassy terrain mixed with metal debris, a few trees and a few roads [5]. For urban terrain, as considered in this paper and illustrated in figure 2, one finds that $\kappa < 0.5$ provides a better fit, especially for extreme values of the random variable - see figure 1. If the texture product model is not used, and homogeneous terrain is assumed, then the pdf has been shown to significantly differ from the measured histogram, [5]. In fact, we see in figure 1 that the model for moderately homogeneous terrain, $\kappa = 1.0$, does not match the urban terrain histrogram very well. If the theoretical pdf does not accurately model the histogram, then reliable CFAR detection fails.

Solving for ν involves estimating the first and second moments from the data then using (29) with $r = 1$ and $r = 2$ to create two equations with two unknowns, namely, σ^2 and ν. Theoretically, if the model was perfect, (29) could also generate three equations with three unknowns thereby allowing the value of κ also to be automatically estimated from the data. The estimates of ν and κ could then be indexed into a map of possible classifications of terrain types to provide contextual information about the terrain being examined.

In the case of $\kappa = 1$, solving (29) leads to the following estimate for ν

$$\hat{\nu} = \frac{2(\hat{I}_2 - \hat{I}_1^2)}{\hat{I}_2 - 2\hat{I}_1^2}, \qquad (30)$$

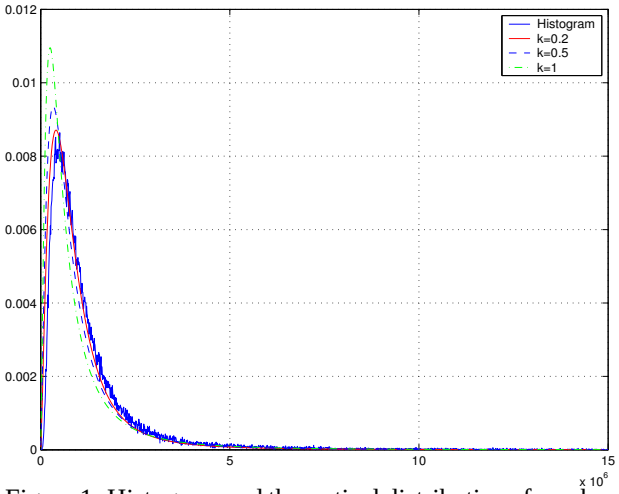

Figure 1. Histogram and theoretical distributions for urban terrain.

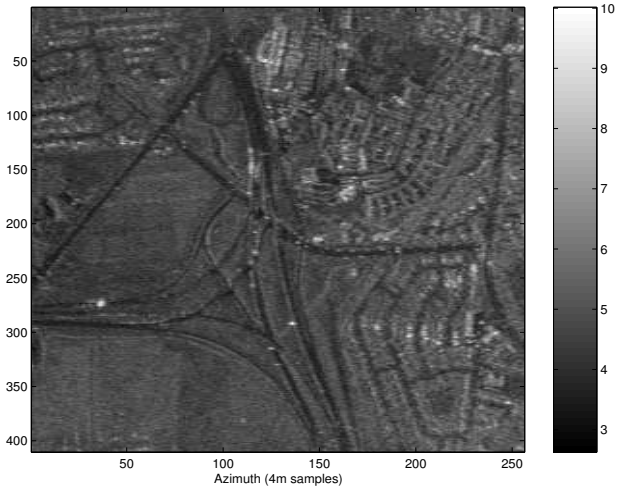

Figure 2. SAR image of Ottawa West.

where the estimated moments are given by $\hat{I}_1$ and $\hat{I}_2$. Depending on the terrain type, the general equation (29), or the specific equation (30) can be used to automatically estimate the parameters of the texture random variable. Either can be computed from a single channel of data.

6. MAXIMUM LIKELIHOOD DETECTION AND PARAMETER ESTIMATION

As discussed in [9, 11], a moving target SCR can be increased by applying a SAR processing filter designed to compress moving targets rather than the stationary terrain. These tailored filters designed under the assumption that the target moves with constant velocity in the slant-range plane with along-track velocity v_x and slant-range velocity v_y can help to detect relatively weak or relatively slow moving targets that are rejected by a DPCA threshold that has to account for bright stationary targets. We propose the following: to construct a filter bank indexed by two candidate velocity variables, $\hat{v}_x$ and $\hat{v}_y$, to pass the SAR data through each of the filters, to test for moving targets using the aforementioned statistical model, and then to analyse the resulting collection of target detections. This filterbank approach provides maximum likelihood estimates of v_y and v_x as the target response maximises at the correct choice for $\hat{v}_x$ and $\hat{v}_y$.

Measured data in this paper were collected using Environment Canada's Convair 580 aircraft configured in its along-track interferometric mode [9]. These data, measuring a scene over West Ottawa in 2001, are illustrated as a SAR image in figure 2.

7. ARBITRATION OF FILTERBANK DETECTIONS

In processed SAR data, a point target impulse response depends on v_x, v_y, $\hat{v}_x$ and $\hat{v}_y$, and x_b, the along-track position of the target when it is in the centre of the beam. For a fixed $\hat{v}_y$, varying $\hat{v}_x$ causes the target to slowly change its x position (along-track dimension) while the target impulse response broadens in the x-direction. Conversely, for a fixed $\hat{v}_x$, varying $\hat{v}_y$ causes the target to move significantly in the x-direction with a decrease in the impulse response power and only a minimal broadening due to defocus [9]. In both cases, only minimal broadening and shifting occurs in the y-direction (the slant-range dimension). For the sake of simplicity, let us assume that the target response manifests at a constant y (no range migration) so that

$$f(x, y) = f_y(x_b, v_x, v_y; x, \hat{v}_x, \hat{v}_y) \qquad (31)$$

Arbitration of the filterbank detections seeks to determine the true beam-centre location of a moving target. This is the broadside location for a side-looking radar and it appears at the point where the filterbank response achieves a maximum, theoretically at $\hat{v}_x = v_x$ and $\hat{v}_y = v_y$. We propose to detect this maximum by using (31) as a matched filter applied to the data produced by the filterbank. Such a scheme provides the advantage of automatically tracking detected targets through the filterbank as the targets displace over $\hat{v}_y$. Otherwise, one would need to locate the position of a given target in the output of each filter, separate this target from neighbouring targets, and ultimately find the filter that produced the maximum response for the given target. In constructing the matched filter, we choose $v_x = v_y = x_b = 0$ because the displacement and the broadening depend, mainly, on $v_y - \hat{v}_y$ and $v_x - \hat{v}_x$ respectively.

The matched filtering of the filterbank data is readily achieved using 3-D FFTs. Once the data have been filtered, the location of a target maximum is determined by seeking local maxima of the function defined by

$$x_t = \max_{\hat{v}_x, \hat{v}_y} F(x, \hat{v}_x, \hat{v}_y), \qquad (32)$$

where $F(x, \hat{v}_x, \hat{v}_y)$ is the output of the matched filtering. Figure 3 shows the location of these maxima. While some

false alarms are still present, the image shows targets on roads. Unfortunately, ground truthing the moving targets over such a large area was not feasible. However, due to non-zero values in the recorded ATI phase, $|\delta| > 0.15$ we highlight, in figure 4 what are probably moving targets; those targets with a large negative phase have been highlighted with a '$\triangleleft$' symbol, those with a large positive phase with a '$\triangleright$' symbol. The positive phase targets, unless phase wrapped, are moving away from the radar while the negative phase targets, unless wrapped, are moving toward the radar.

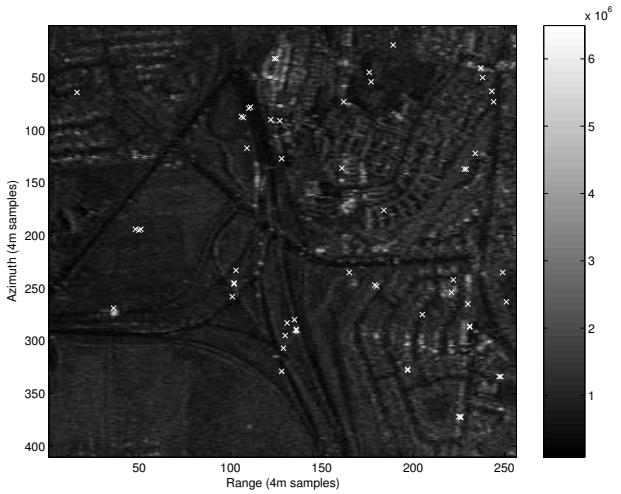

Figure 3. All detected moving targets.

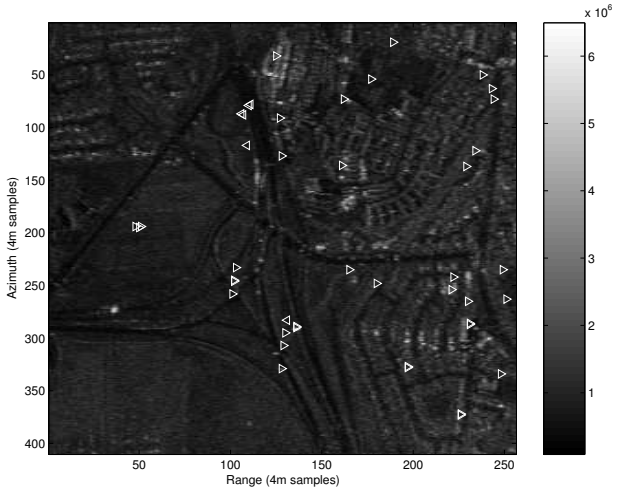

Figure 4. $|\delta| > 0.15$ moving targets, negative phase denoted by '$\triangleleft$', positive phase denoted by '$\triangleright$'.

8. CONCLUSION

The proposed pdf for the texture component of the product model, commonly used for heterogeneous terrain, fits data collected over urban areas very well. Our paper implements this pdf and applies CFAR rules using DPCA as the detection metric. The number of false alarms detected seems to agree with the number predicted theoretically. Unfortunately, achieving the CFAR reduces the detection rate for low probabilities of false alarm. To enhance the detection, this paper proposes to process the SAR data with filters designed to compress non-zero velocity targets. A filterbank indexed by two filtering parameters, namely the candidate across-track velocity and the candidate along-track velocity, produces a set of target detections that we subsequently analyse to extract estimates of the velocity and position of the targets. Theoretically, the target power peaks at the correct choice for the velocity parameters. This paper proposes to locate the maximum target power over the possible filterbanks by matching the filterbank output with the expected trajectory of a point target through the filterbank space. This we achieve by using a 3-D matched filter. The output of the matched filtering is a data set in which local maxima represent estimates of the position and velocity of moving targets.

Future work will apply the texture pdf model of this paper, but use a different GMTI detection metric. Among the possible candidates are the hyperbolic detector and the ATI phase as these have been shown to possess greater probabilities of detection than DPCA in heterogeneous terrain [11, 12].

9. REFERENCES

[1] C. H. Gierull. Statistics of SAR interferograms with application to moving target detection. Technical Report TR 2001-045, Defence Research and Development Canada, July 2001.

[2] C. H. Gierull. Unbiased coherence estimator for SAR interferometry with application to moving target detection. *Electronics Letters*, 37(14):913–915, July 2001.

[3] C. H. Gierull. Moving target detection with along-track SAR interferometry. Technical Report TR 2002-084, Defence Research and Development Canada, January 2002.

[4] C. H. Gierull and C. E. Livingstone. *The Applications of Space-Time Processing*, chapter SAR GMTI concept for RADARSAT-2. IEE Publishers, 2003.

[5] C. H. Gierull, Christoph. Statistical analysis of multilook SAR interferograms for CFAR detection of ground moving targets. *IEEE Trans. Geosci. and Rem. Sens.*, 42(4):691–701, April 2004.

[6] I. S. Gradshteyn and I. M. Ryzhik. *Table of Integrals, Series and Products*. Academic Press, New York, sixth edition, 2000.

[7] I. R. Joughin, D. P. Winebrenner, and D. B. Percival. Probablility density functions for multilook polarimetric signatures. *IEEE Trans. Geosci and Rem. Sens.*, 32(3):562–574, May 1994.

[8] J. S. Lee, A. R. Miller, and K. W. Hoppel. Statistics of phase difference and product magnitude of multi–look processed gaussian signals. *Waves in Random Media. IOP Publishing Inc. London UK*, 4:307–317, 1994.

[9] C. E. Livingstone, I. Sikaneta, C.H. Gierull, S. Chiu, A. Beaudoin, J. Campbell, J. Beaudoin, S. Gong, and T.A. Knight. An airborne synthetic aperture radar (SAR) experiment to support RADARSAT-2 ground moving target indication (GMTI). *Can. J. Rem. Sens.*, 28(6):1–20, 2002.

[10] P. C. B. Phillips. The true characteristic function of the F-distribution. *Biometrica*, 69(1):261–264, 1982.

[11] I. C. Sikaneta. *Detection of Ground Moving Objects with Synthetic Aperture Radar*. PhD thesis, University of Ottawa, December 2004.

[12] I. C. Sikaneta and J-Y. Chouinard. Eigendecomposition of the multi-channel covariance matrix with applications to sar-gmti. *Euro. J. Sig. Proc.*, (84):1501–1535, 2004.

[13] M. R. Spiegel. *Theory and Problems of Probability and Statistics*. McGraw-Hill, New York, 1994.

[14] R. A. J. Tough, D Blacknell, and S. Quegan. A statistical description of polarimetric and interferometric synthetic aperture radar data. *Proc. R. Soc. Lond., A. Math. Phs. Sci*, A(449):567–589, 1995.